Innovative monochromatic x-ray source for high-quality and low-dose medical imaging

Eric H. Silver[a)] and Seth D. Shulman
Imagine Scientific, Inc., 90 Kerry Place, Norwood, MA 02062, USA

Madan M. Rehani
Massachusetts General Hospital, Boston, MA 02114, USA

(Received 15 October 2020; revised 14 December 2020; accepted for publication 14 December 2020; published 12 February 2021)

Purpose: An estimated 377 million diagnostic and interventional radiological exams are performed annually in the United States and approximately 4 to 5 billion globally. All use x-ray tubes that emit x-rays over a broad energy band, a technology that is more than a century old. Only a small fraction of the radiation is useful for imaging while the remaining fraction either increases the radiation dose received by the patient or degrades the image. Monochromatic x-rays can provide lower dose images in many of these radiological applications while maintaining or improving image quality. We report the development of the first monochromatic x-ray source suitable for low-dose, high-quality imaging in the clinic and demonstrate its first application and performance with mammography phantoms.
Methods: X-ray fluorescence was used to generate monochromatic x-rays with selectable energies from 18 to 60 keV. This patented technology was incorporated into a laboratory prototype of a monochromatic x-ray mammography system. Image quality was evaluated as a function of radiation dose in standard breast phantoms using the signal-to-noise ratio (SNR) measured for high and low contrast masses and microcalcifications. Spatial imaging properties were assessed from these images as well as from modulation transfer function (MTF) analysis. Measurements using an iodine contrast agent were also performed. The results were compared to those obtained using a commercially available, conventional x-ray mammography system.
Results: Our prototype system reduced radiation dose by factors of five to ten times for the same SNRs as obtained from the conventional system. This performance was demonstrated in phantoms simulating a wide range of lesion sizes and microcalcifications in a variety of breast thicknesses. The high SNRs for very thick breast phantoms provide evidence that screening with less breast compression is possible while maintaining image quality. Contrast-enhanced digital mammography (CEDM) with monochromatic x-rays was shown to provide a simpler and more effective technique at substantially lower radiation dose. The MTF value at 20% was 9 lp/mm.
Conclusions: The monochromatic x-ray system is more sensitive for imaging a wide range of breast sizes and compositions than conventional broadband mammography. High image quality and lower dose are its hallmarks. It also makes CEDM much more effective than current methods developed for use with conventional broadband mammography systems. [https://doi.org/10.1002/mp.14677]

Key words: monochromatic x-rays, image quality, mammography, phantoms, radiation dose

1. INTRODUCTION

An estimated 377 million diagnostic and interventional radiological exams are performed annually in the United States.[1] All use x-ray tubes that emit x-rays over a broad energy band, a technology that is more than a century old. Scientists have utilized different spectral filtering strategies to shape this broadband Bremsstrahlung spectrum in efforts to remove x-rays that do not contribute to the image formation, degrade image quality, and increase the radiation dose received by the patient. Dose reduction is important because recent studies show that many patients receive multiple imaging exams resulting in cumulative radiation doses at which radiation damage is known to occur.[2–5]

A monochromatic source of radiation for use in the clinic would reduce the dose and, if capable of providing selectable energies, could optimize the signal-to-noise (SNR) of the image and may help to spectroscopically determine in vivo the chemical composition of tumors and surrounding tissue.[6–11] To date, research studies demonstrating the advantages of monochromatic x-ray imaging have been carried out primarily using either large synchrotron facilities or traditional broadband x-ray tubes.[12–16] For examples, experiments with crystal monochromators[15] coupled to synchrotrons concluded that energies between 20 and 26 keV are optimal for breast imaging. Compared to measurements with conventional systems, these investigations showed that dose reductions of about six times could be achieved at 22 keV for a 5 cm thick phantom while maintaining comparable SNR. Higher throughput monochromators using multilayer structures instead of conventional Bragg crystals offer possibilities of monochromatic imaging using conventional broadband

x-ray sources instead of synchrotrons. Measurements with multilayers that produce monochromatic lines at 18 and 21.5 keV are described in the literature.[17,18] In particular, narrow band emission centered at 21.5 keV showed a 12-fold reduction in dose on a 4.5 cm thick breast phantom compared to that obtained using a tungsten-based x-ray tube while achieving 1.85 times improvement in the SNR. The system used for the latter experiments also demonstrated a spatial resolution of 7 lp/mm as defined by the 10% level of its measured MTF.[17]

Neither of these technologies are suitable for general use in the clinic. Synchrotrons are large, expensive, shared research facilities, and crystal/multilayer monochromator systems coupled to standard x-ray tubes cannot produce an x-ray beam with a sufficiently large field-of-view and intensity for routine clinical imaging. Rather, they require scanning the monochromatic, fan-shaped beam to image a large field-of-view.

We have developed a prototype x-ray tube with a properly shaped, monochromatic x-ray beam suitable for many medical imaging tasks and extensively tested its imaging characteristics in mammography phantoms.

2. MATERIALS AND METHODS

2.A. The monochromatic X-ray tube*

2.A.1. Design and spectral characteristics

The design of our monochromatic x-ray tube is schematically shown in Fig. 1. Bremsstrahlung and characteristic line emission from a conically shaped anode made of gold-coated tungsten fluoresce a compact target. These targets take the form of solid cones or single or double, thin-foil cones. An example of the fluorescence spectrum emitted by a compact target of tin (Sn) is shown in Fig. 2. It consists of two monochromatic emission lines, one very strong Kα line at 25.27 keV and a much weaker Kβ line at 28.49 keV. The voltage between the cathode and anode was 80 kV in this example. The spectrum was measured with a Cadmium Telluride photon counting detector[19] with a thickness of 1 mm and an area of 25 mm^2. A 2 mm thick tungsten disk with a 1 mm diameter aperture was placed over the detector to limit the count rate and maintain the acquisition dead time to <2%. The energy spectrum was calibrated with a series of radioactive sources spanning the 6 to 88 keV range. The energy resolution at 25 keV is about 0.75 keV.

We define the percent monochromaticity, *M*, as the combined integrated energy of the Kα and Kβ lines divided by the integrated energy in the entire spectrum and multiplied by 100. The tube generates x-rays with a monochromaticity of 95% or higher. For the tin target, as shown in the inset in the top right of Fig. 2, only a small amount (~4%) of the anode bremsstrahlung spectrum reaches the detector, and the measured monochromaticity was 96%.

2.A.2. Input power and intensity of monochromatic x-rays

The shape, size, and mass of the stationary anode are ideal for high power applications. Electrons liberated from the toroidal cathode travel along trajectories that terminate on the anode in a locus of points that maps out an annulus. This relatively large area distribution of electrons minimizes localized electron heating in the anode. The current version of the source operates continuously at a total input power of 1.6 kW with a power density on the anode of 400 W/cm^2. For comparison, modern high power rotating anode conventional x-ray tubes operate with at least input power densities 16 times higher. The stationary anode is easily water cooled to maintain its temperature within the range of 20–30°C. The tube housing is 34 cm long and 11 cm in diameter and has been engineered to fit into a cylindrical package that can be easily contained in the volume of existing commercial mammography systems.

In addition to the input power, the monochromatic flux is governed by the surface area of the conical fluorescence target and its absorption efficiencies for the incident Bremsstrahlung radiation and the escaping fluorescent x-rays. The conical base diameter and peak height determine the surface area and the effective spot size. Together with the source-to-detector distance, these parameters influence the ultimate spatial resolution of the imaging system which is discussed below. For fixed input power, there is usually a tradeoff between flux and spatial resolution and depends on the specific imaging application. For the mammography studies described in this paper, a single, conical foil target with base diameter of 4 mm, height of 7.45 mm that is truncated to a height of 5.5 mm (apex angle of 30 deg), and thickness of 35 microns was used. The conical foil is inverted with its apex directed to the interior of the tube. This orientation and thickness optimizes the absorption of the incoming broadband continuum x-rays while minimizing the absorption of the escaping fluorescent x-rays.

Referring to the spectrum in Fig. 2, the combined intensity of Sn Kα and Kβ is 3.5×10^7 $keV/cm^2/mAs$ at the center of the relatively flat emission profile shown in Fig. 3. The source-to-detector distance is 76 cm which is used for all of the imaging measurements discussed below. This line flux represents the total photon counts in the respective Sn Kα and Kβ peaks shown in Fig. 2. The combined strength of the two lines is used for imaging and for brevity will be referred to by their Kα energies in the text below.

It is instructive to point out that these monochromatic line intensities are consistent with estimates of the line flux expected from the tube. Briefly, the efficiency, ϵ, for Bremsstrahlung production in a thick target for an incident electron beam is approximately $V \times Z \times 10^{-6}$, where V is the accelerating potential in kilovolts, and Z is the atomic number of the thick target.[20] ϵ equals 6.3×10^{-3} for the

*Note that the word *tube* is used when discussing the device in technical terms and the word *source* is used when the device is discussed in conjunction with the imaging system.

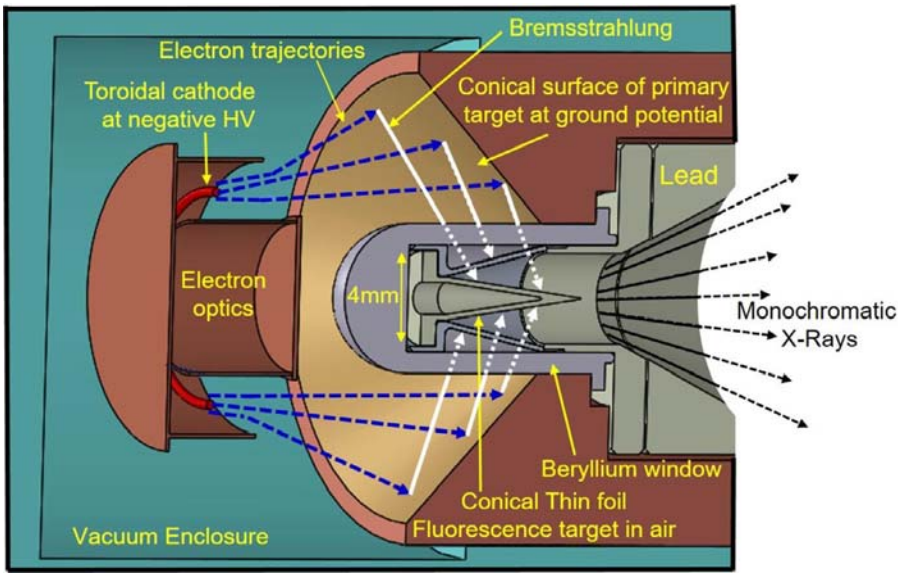

FIG. 1. A three-dimensional section of the prototype monochromatic x-ray generator. A toroidal cathode at negative HV emits electrons that are guided by electron optics along trajectories, shown schematically in dark blue, that end on the inside surface of the conical primary target (anode). Broadband bremsstrahlung x-rays from the conical primary target, shown schematically in white, pass through a beryllium window that seals the vacuum enclosure from atmospheric pressure. These x-rays interact with the conical secondary metal target to produce fluorescence x-rays with the desired monochromatic energy. [Color figure can be viewed at wileyonlinelibrary.com]

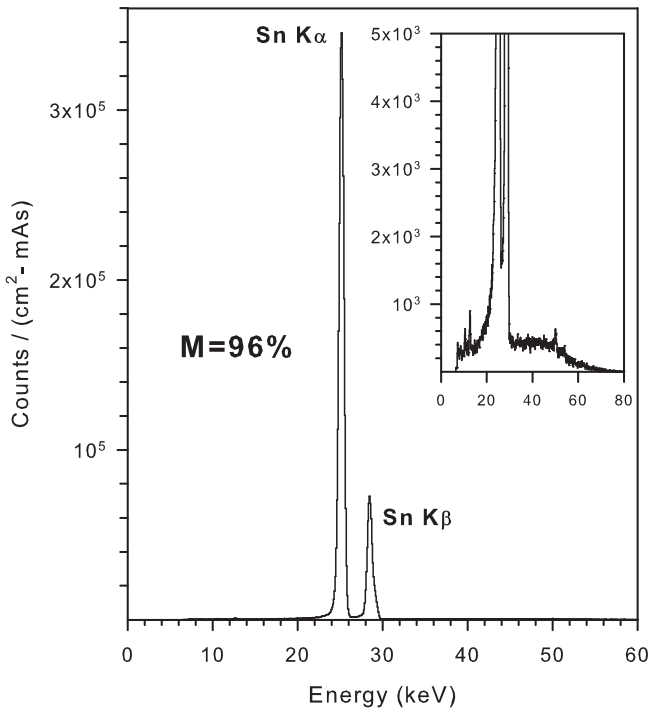

FIG. 2. The fluorescence spectrum from a target of tin (Sn) emitted by the prototype. The monochromaticity is 96%.

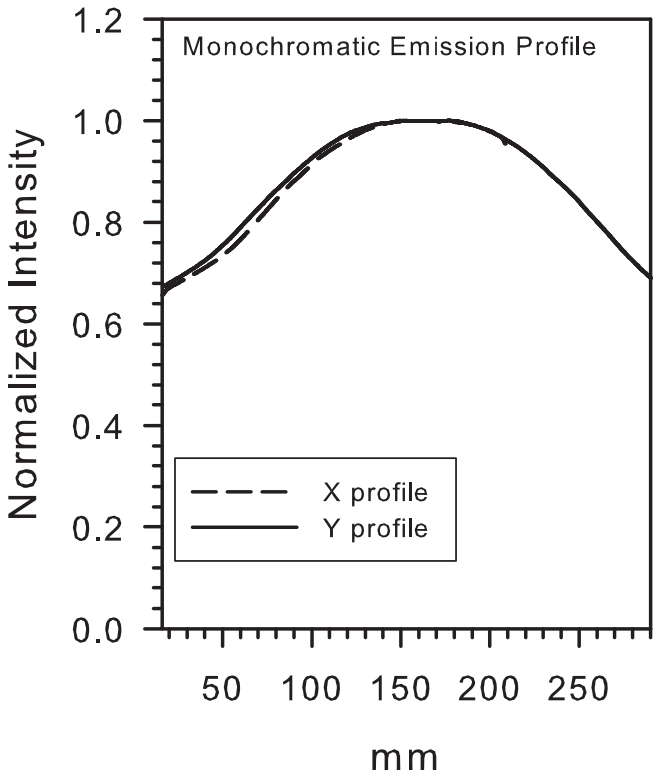

FIG. 3. The orthogonal emission profiles.

80 kV potential used to accelerate the electrons in this example and Z = 79 for the gold anode. Consequently, the 1.6 kW of input power dissipated in the anode by the 20 mA electrons produces 10 W of Bremsstrahlung radiation. The solid angle subtended by the thin foil tin cone at the anode is approximately 0.14 steradians. Only Bremsstrahlung photons above the tin absorption edge at 29 keV are useful for inducing x-ray fluorescence in the thin foil cone and represent about 16% of the Bremsstrahlung emission with an endpoint energy of 80 keV according to our modeling of the broadband spectral distribution. On average, the probability that these Bremsstrahlung photons are absorbed in the 35-micron-thick tin foil cone and produce monochromatic tin fluorescence photons which escape the

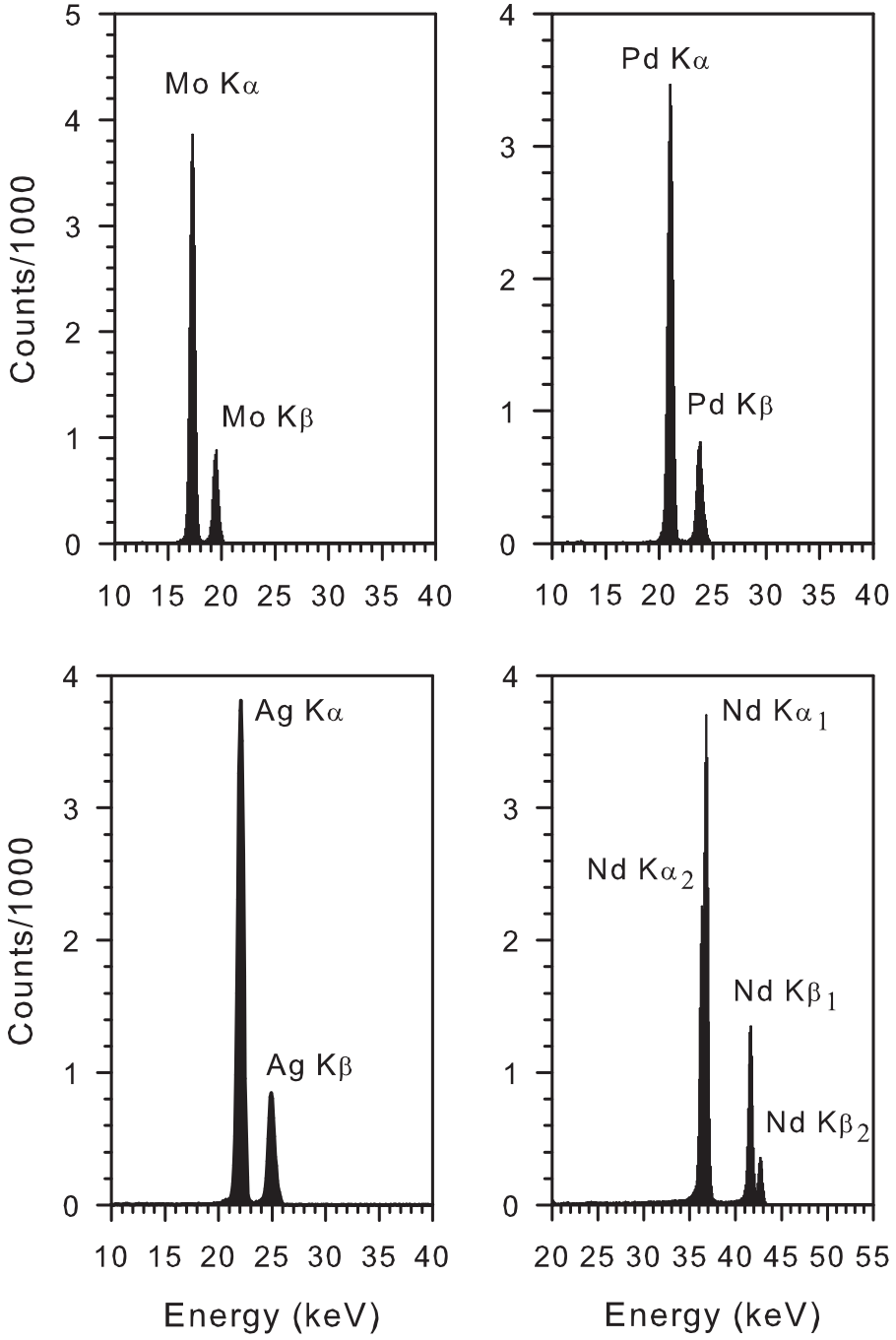

FIG. 4. Additional examples of monoenergetic fluorescent x-ray lines used for imaging. Top left: molybdenum (Mo); top right: palladium (Pd); bottom left: silver (Ag); bottom right: neodymium (Nd).

foil is estimated to be 17% for x-ray energies between 29 and 80 keV. This estimate is based on our own calculations and is similar to those for higher energy Bremsstrahlung spectra.[21] Accounting for these factors and the fluorescence yield for tin of 0.88 means that 0.038 W or 2.4×10^{14} keV/s of energy in the Sn K lines are emitted. The flux at the detector is therefore 1.4×10^{8} keV/cm^2/mAs for 20 mA. This approximation is consistent with our measurement of 3.5×10^{7} keV/cm^2/mAs to within a factor of 4, as well as with the value of 3.8×10^{7} keV/cm^2/mAs obtained with a Monte Carlo simulation that we developed to optimize the design of the x-ray tube.

The monochromatic energy can be selected by changing the material of the fluorescence target. Molybdenum, palladium, silver, and antimony generate similar monochromatic fluxes and all are potentially useful in mammography. Three of these are displayed in Fig. 4 and their energies are listed in Table I. Higher energy monochromatic fluxes can be generated using acceleration voltages ≥80 keV and with target materials such as neodymium, samarium, dysprosium, tungsten, and gold. Their energies are also listed in Table I and the spectrum from a neodymium target is displayed in Fig. 4. The tube allows for easy manual exchange of the secondary target to select the monochromatic energy because the target

TABLE I. Examples of potential elements and their respective K x-rays that can be fluoresced.

	Energy (keV)	
Element (Z)	Kα1	Kβ1
Molybdenum (42)	17.48	19.61
Palladium (46)	21.18	23.82
Silver (47)	22.16	24.94
Tin (50)	25.27	28.49
Antimony (51)	26.36	29.73
Neodymium (60)	37.36	42.27
Samarium (62)	40.12	45.41
Dysprosium (66)	45.99	52.12
Tungsten (74)	59.32	67.24
Gold (79)	68.8	77.98
Uranium (92)	98.43	111.3

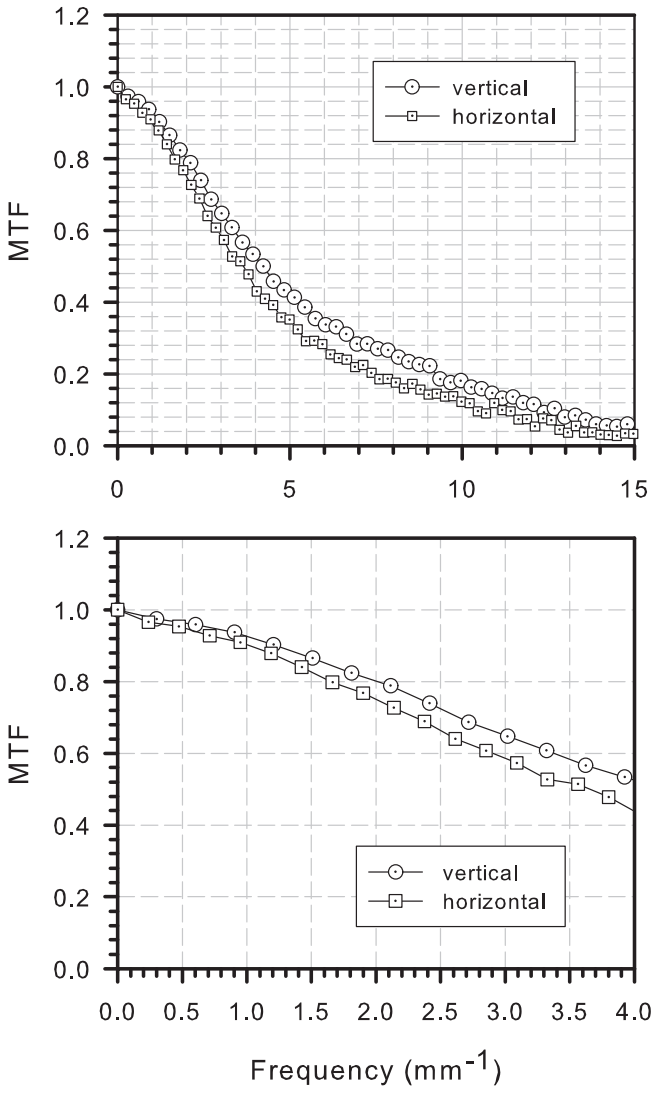

FIG. 5. The modulation transfer function measured with silver K x-rays.

is located outside the vacuum of the x-ray tube. Automated target replacement is under development. The tube technology has received a number of international patents.[22–31]

2.A.3. Prototype mammography system

A laboratory prototype mammography system has been assembled using the monochromatic x-ray source and a 24×30 cm^2 amorphous selenium detector with 85 micron pixel pitch[32] at a distance of 76 cm from the source. The imaging properties of the system were assessed by measuring the effective spot size, the modulation transfer function (MTF) and by imaging a standard 4.5 cm thick breast phantom. The effective projected spot size of the fluorescence target was determined to be ~3 mm by imaging the monochromatic source through a 25 micron pinhole in a tungsten disk placed at 1/3 of the distance to the imaging detector.

The MTF was measured using a variant of the opaque edge test originally suggested by Illers et al.[33] and formally adopted by the IEC Standards Committee in the Standard IEC 62220-1 published in October 2003.[34] The MTF for the monochromatic system is shown in Fig. 5. The value of 0.2 at 9 lines/mm is comparable to commercial systems with direct detector systems and better than flat panel detectors.[33] This is further substantiated by measurements of line-pair resolution as shown in Fig. 6. The figure shows intensity scans through line-pair targets embedded in the 4.5 cm thick phantom. The spacing of the line-pair targets ranges from five lines per millimeter up to ten lines per millimeter in the Figure. The top 4 figures show that the grayscale profiles for 18, 21, 22, and 25 keV energies can discern alternating intensity structure up to nine lines per millimeter which is consistent with a spatial resolution FWHM of 110 microns. The 18 keV energy can still discern structure at ten lines per millimeter. The bottom profile in Fig. 6 is the grayscale intensity scan through the same line-pair ensemble using a commercial broadband mammography system.[35] Its ability to discern structure reaches eight lines per millimeter.

2.B. Phantom studies with a laboratory prototype system

Imaging measurements of four breast phantoms were taken with the prototype monochromatic system and with a commercially available mammography system for comparison.[35] The images represent the raw grayscale data recorded by the detector in each system and only incorporate detector electronics and system flat-field corrections. In addition to comparing the spatial imaging quality, we also used the SNR as the appropriate metric to compare the detectability of the two instruments. For the SNR estimates reported throughout this paper, $\mathrm{SNR} = (\mathrm{Nb} - \mathrm{Nm})/\sigma$, where Nb and Nm are the integrated gray counts in n pixels of the background and n

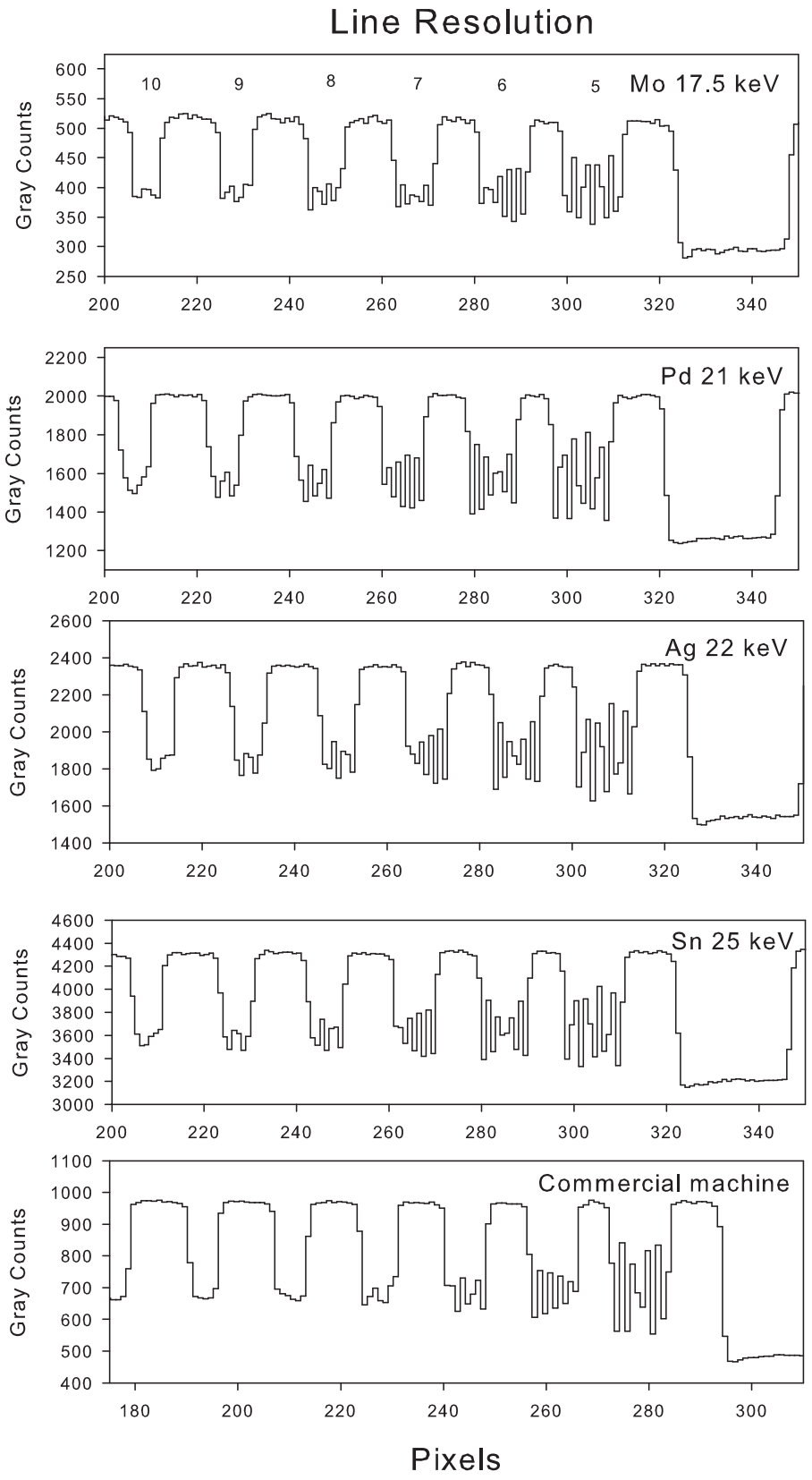

FIG. 6. The line-pair resolution of the monochromatic source measured at various monochromatic energies and for a broadband commercial system.

pixels of the embedded feature of interest; σ is the standard deviation of the integrated gray count values in the background.

The SNR was estimated for thick, high contrast step wedges in a 4.5 cm thick CIRS[36] Model 011a phantom while the 4.1 cm thick CIRS Model 086 ACR (American College

of Radiology) Digital Mammography Accreditation Phantom was used for comparing performance on thin, low contrast masses. We simulated 7.1 cm and 9 cm thick compressed breasts by stacking three, 1 cm thick, soft tissue-equivalent slabs on top of the Model 086 phantom and also by stacking a 4.5 cm thick CIRS Model 015 Mammographic Accreditation Phantom on top of the CIRS Model 011a. Measurements using an iodine contrast agent were also performed and we compared the spatial resolution properties of each system by imaging simulated microcalcifications composed of Al_2O_3, $CaCO_3$ and precision glass spheres. All measurements with the monochromatic prototype were conducted without an antiscatter grid.

For conventional broadband mammography, conversion factors derived from Monte Carlo simulations of breast models that relate the incident radiation flux to the glandular dose are widely used for estimating the mean glandular dose (MGD).[37–43] The differences in doses reported by the most common simulations can vary by as much as 19%.[44] This variability is inherent in the MGDs reported by different vendors of mammographic systems who choose to use one set of factors over another in their algorithms. For the comparison images from the conventional, broadband mammography system, we used the MGD provided in its DICOM (Digital Imaging and Communications) header. All of the measurements with the conventional machine used a rhodium anode, a 50 micron rhodium filter and incorporated a reciprocating antiscatter grid with a pitch of 36 lines per cm and 5:1 grid ratio. The specific operating parameters (e.g., kVp, emission current, etc.) are indicated for each image below.

Several Monte Carlo studies can predict the MGD for incident x-rays with an arbitrary spectral distribution.[41–43] These are particularly useful for estimating the MGD for the monochromatic x-ray spectra produced by our system. We have corroborated that the MGD values predicted by the simulations are consistent with our analytical methods and those used for measurements made with monochromatic beams produced with synchrotron sources to within 15%.[14,15]

3. RESULTS

3.A. SNR comparisons in thin and thick breast phantoms

3.A.1. High contrast masses

Images of a 4.5 cm thick CIRS 011a breast phantom (50% glandular: 50% adipose equivalent) obtained with the prototype system using monochromatic x-rays at 22 keV (silver) and 25 keV (tin) and with the conventional unit are shown in Fig. 7. This phantom includes 1 cm thick step wedges (shown vertically) of differing simulated breast densities ranging from 100% adipose to 100% glandular. For these flat, relatively large area uniform step wedges, we chose an area of 5 mm × 5 mm to calculate the SNR.

The SNR measured by the conventional mammography system for the 100% glandular block was 403 for a mean glandular dose of 1.26 mGy at 29 kVp. A slightly higher SNR was measured, 460–500, with the monochromatic prototype, and the doses and exposure times were estimated to be 0.27 mGy (14 s) at 22 keV and 0.23 mGy (14.5 s) at 25 keV. For equal SNR to the conventional unit, the monochromatic doses would drop to 0.18 mGy (9.3 s) and 0.17 mGy (11 s) for the 22 and 25 keV images, respectively, an ~85% reduction.

The advantage of monochromatic x-rays becomes even clearer when we consider imaging thick breasts. Using the 9 cm compressed breast phantom described above (ACR Model 18-222 + CIRS Model 011a), Fig. 8 shows the image from the conventional system with a SNR of 138 for the 100% glandular block at a dose of 2.75 mGy at 30 kVp. Our monochromatic system, by comparison, obtained a SNR of 364 at a dose that is 4.2 times lower, only 0.65 mGy (100 s). The SNR was estimated for a 3.8 × 3.8 mm area to avoid blemishes and a crack in the wax insert of the CIRS Model 015 phantom on top of the CIRS Modell 011a. The SNR of the prototype is 749 when extrapolated to the conventional system dose of 2.75 mGy; it is ~5 times higher than the SNR (138) of the conventional system. To equal the monochromatic performance at 2.75 mGy, the required dose from the conventional system would be $2.75 \times (749/138)^2 = 81$ mGy since the dose scales with the square of the SNR.

3.A.2. Low contrast masses

The CIRS Model 086 ACR phantom was used for imaging studies of low contrast masses. This phantom approximates a 4.1 cm thick compressed breast and combines a 4.1 cm thick slab of PMMA (polymethyl methacrylate) (50% glandular: 50% adipose equivalent) with a 0.7 cm thick wax insert which contains a variety of test objects that simulate tissue fibers (nylon monofilaments), microcalcifications (glass spheres), and thin, low contrast lesions (masses of 10% adipose: 90% glandular equivalent).

We compared images from both the conventional and monochromatic system over a range of doses. Exposures of 1.31 and 3.62 mGy were taken with the conventional system. Images were taken with the monochromatic system at 0.53, 1.3, and 3.45 mGy using the Ag (22 keV) target and 0.55, 0.83, 1.1, and 2.2 mGy using the Sn (25 keV) target. In Fig. 9(a), we show the 3.62 mGy conventional image compared to the 0.55 mGy Sn monochromatic image.

The fibers, microcalcifications, and low contrast lesions are observable in both images. To quantify the comparisons for the low contrast lesions outlined in the dashed yellow rectangles, the SNR is plotted in Fig. 9(b) for the range of radiation doses used in the experiments. The exposure times are also listed in the legend of Fig. 9(b) for each measurement. The conventional system requires 4.5 times the dose for the 1 and 0.75 mm thick lesions and six to eight times the dose for the lesions with thicknesses of 0.5 to 0.2 mm to produce the same SNR as that of monochromatic system.

The monochromatic system also demonstrates superior SNR at lower dose for low contrast masses in a 7.1 cm thick

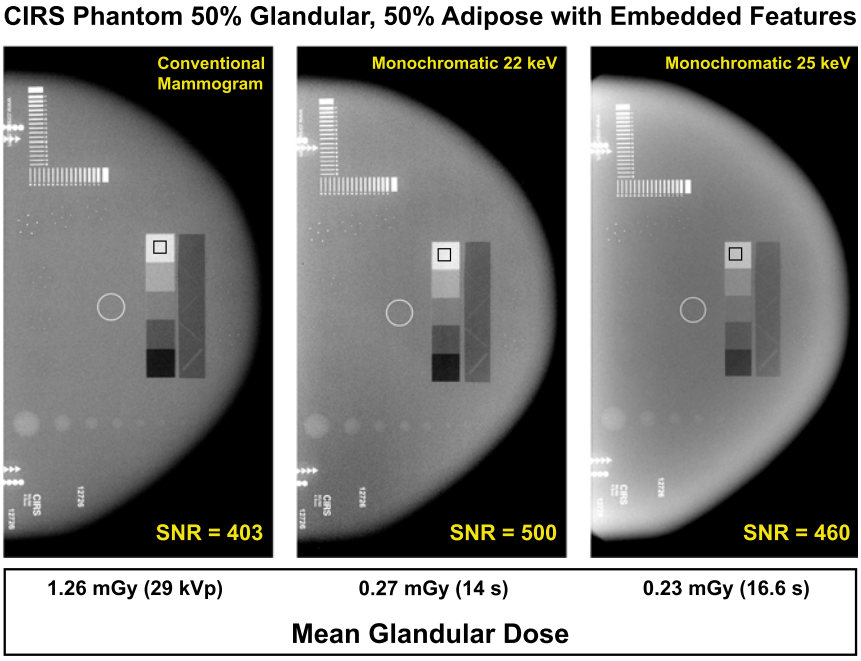

FIG. 7. A 4.5 cm thick breast phantom imaged with a conventional mammography unit and with 22 and 25 keV monochromatic x-rays from our prototype. The SNR for the 100% glandular step wedge is calculated for the 5 mm × 5 mm square outlined in black. [Color figure can be viewed at wileyonlinelibrary.com]

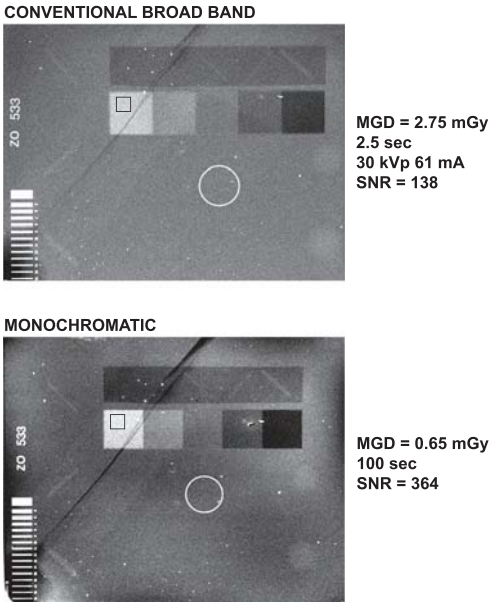

FIG. 8. Images of a 9 cm composite breast phantom made with the conventional unit and the prototype monochromatic x-ray system at 25 keV. The SNR is estimated for the 3.8 mm × 3.8 mm squares outlined in black in the 100% glandular step wedge.

breast phantom. Images for the conventional system were acquired at doses of 2.0 and 3.6 mGy and for the monochromatic system at 0.43, 0.89, 1.45, and 2.9 mGy as shown in Fig. 10. Comparing the conventional broadband system at 3.6 mGy to the monochromatic instrument at 0.89 mGy, the broadband machine requires four times the dose to equal the monochromatic SNR for lesion thicknesses from 1mm to 0.38 mm and five to six times for the 0.25 and 0.2 mm thick lesions. The monochromatic system demonstrates a factor of 4.65 reduction in dose over the full range of thicknesses when comparing its SNRs at 0.43 mGy to those at 2 mGy for the broadband instrument.

3.A.3. Microcalcifications

Figure 11 compares the monochromatic system performance at 25 keV with the conventional mammography system for $CaCO_3$ microcalcifications with diameters of 400, 270, and 230 μm, respectively, in the 4.5 cm thick phantom. The grayscale profiles represent the measured intensities along the yellow lines drawn through two microcalcifications of the 400 and 230 μm ensembles and show the absorption of the $CaCO_3$ specs relative to the background. The peaks in each grayscale profile were fit with a Gaussian distribution plus a baseline. The FWHM of each Gaussian distribution is noted by the horizontal arrows on both sides of the peaks and is a measure of the spatial resolution. The image size of the nominal 400 micron diameter microcalcification is identical for both systems, whereas the image diameter of the nominal 230 micron microcalcification is 10% larger for the monochromatic system compared to the broadband unit. The MGD and the SNR for each set of images are also given. If the MGD for the monochromatic images is increased to the value of the broadband system (1.26 mGy), the corresponding SNR for the 400 and 230 μm microcalcifications would increase by ~2.2 times to 194 and 71, respectively, 2.5–3 times the SNR of the broadband system.

Figure 12 shows a similar comparison of the monochromatic and conventional systems for 230 μm $CaCO_3$

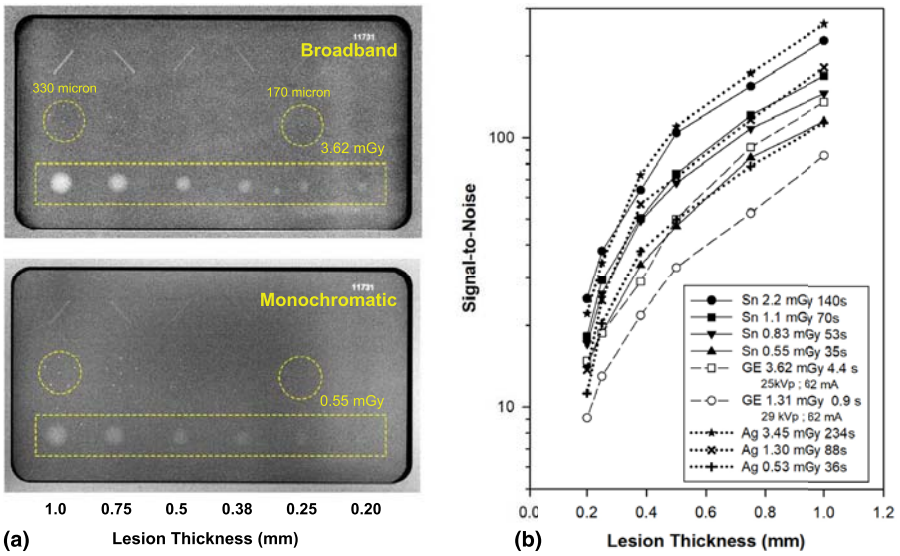

FIG. 9. (a) Images of the 4.1 cm ACR 086 phantom obtained with the conventional unit at 3.62 mGy (top) and the prototype using 25 keV x-rays at 0.55 mGy (bottom). (b) The signal-to-noise ratio of the simulated low contrast lesions measured with the prototype (solid symbols) and the conventional unit (open symbols) for a range of doses. [Color figure can be viewed at wileyonlinelibrary.com]

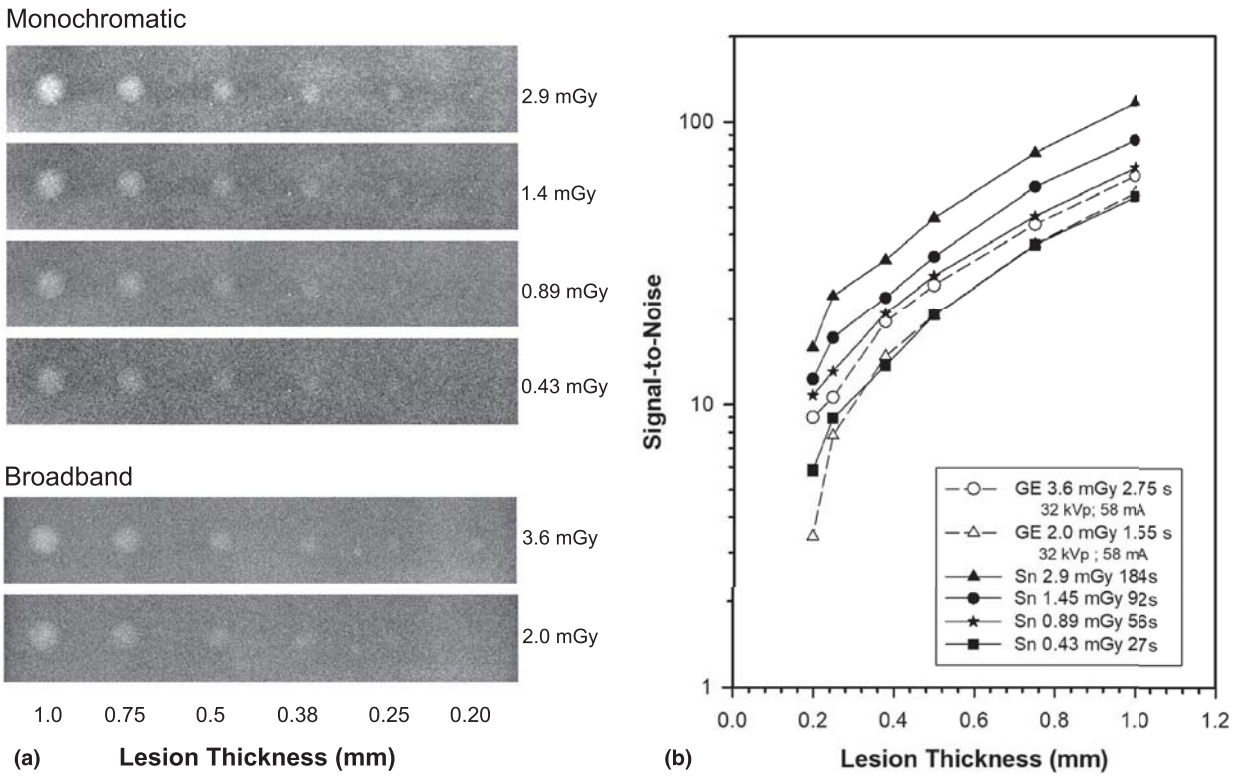

FIG. 10. (a) Images of the 7.1 cm composite phantom obtained with the prototype at 25 keV and with the conventional broadband unit for a range of doses. (b) The signal-to-noise ratio of the simulated low contrast lesions measured with the prototype (solid symbols) and the conventional unit (open symbols) for a range of doses.

microcalcifications in a 9 cm thick phantom. The monochromatic SNR value of 24 is 1.6 times larger than the SNR for the conventional unit, *but* the monochromatic SNR is obtained at 0.65 mGy. If the monochromatic MGD is increased to the 2.75 mGy delivered by the conventional unit, the SNR would be 49, 3.3 times that of the conventional unit.

Imaging the glass spheres in the ACR 086 phantom further illustrates the potential diagnostic capability of the monochromatic system. Images of a series of spheres with diameters decreasing from 330 μm to 170 are shown in Fig. 13. The SNRs measured by the monochromatic prototype for these simulated microcalcifications are similar to

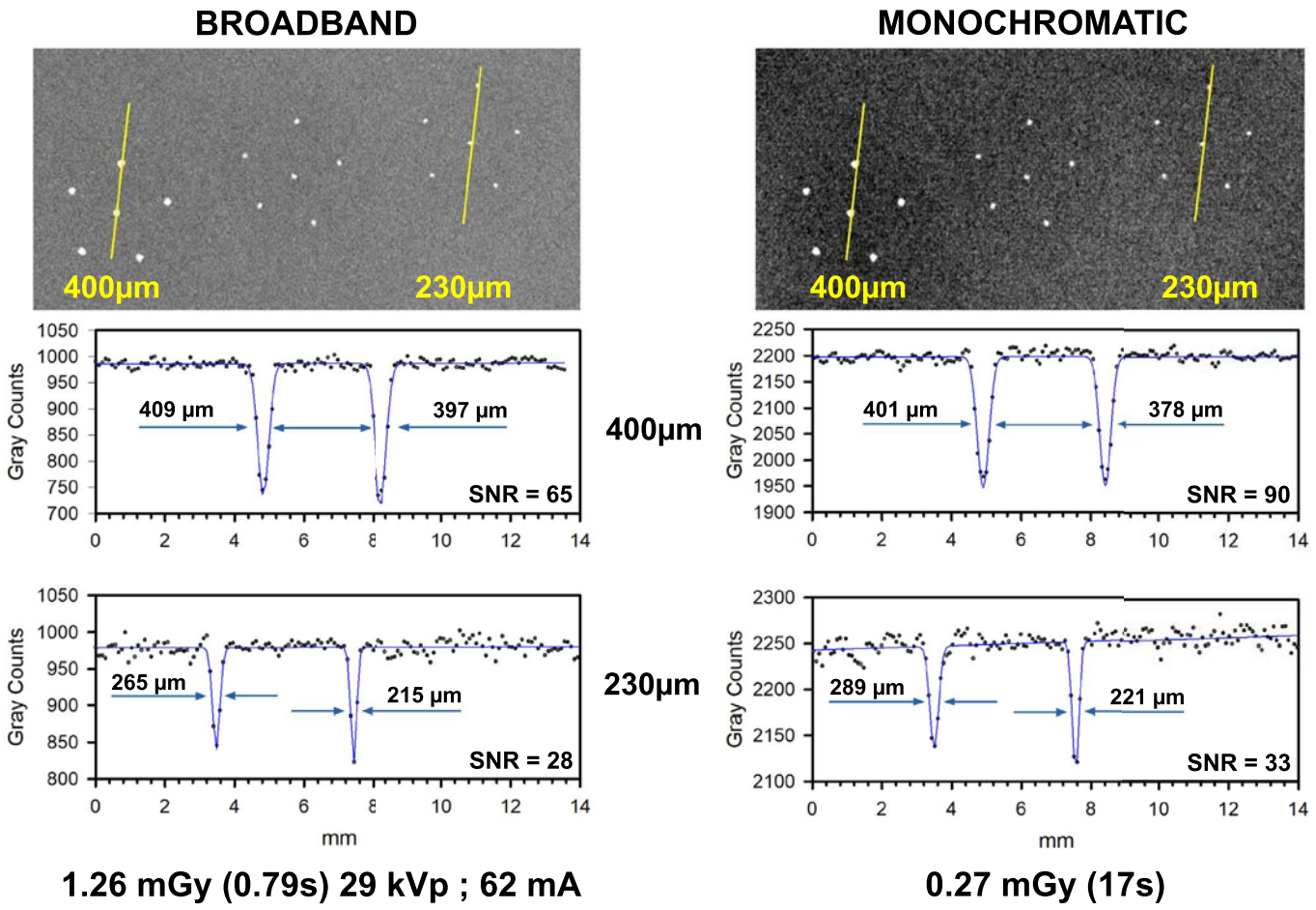

FIG. 11. The intensity profiles of 400 micron and 230 micron diameter $CaCO_3$ microcalcifications in the Model 011a, 4.5 cm phantom measured by the broadband system and the monochromatic prototype at 25 keV. The spatial resolution is defined by the FWHM of the Gaussian distribution fit to the peaks. The signal-to-noise ratio of the prototype at 25 keV is also compared to the conventional unit. [Color figure can be viewed at wileyonlinelibrary.com]

those of the conventional system but imaged at 4.4 times lower dose. Similar improved performance is demonstrated in Fig. 14 for the 7.1 cm thick phantom. Images of the glass spheres are compared between the conventional system at 3.6 mGy and the monochromatic system at 1.45 and 2.9 mGy for the 170 and 330 µm diameter spheres, respectively. The SNR values are shown in the top bar chart. The bottom bar chart extrapolates the dose that the conventional unit would require to equal the SNR achieved by the monochromatic system at 2.9 mGy. The conventional unit doses would be 17 and 13 mGy for the 170 and 330 µm diameter spheres, respectively.

3.B. Contrast enhancement

In contrast enhanced digital mammography (CEDM) as currently practiced with broadband systems, a contrast agent is usually administered to the patient prior to image acquisition with low energy (e.g., 26–32 kVp) and a high energy spectra (e.g., 45–49 kVp). The low energy image is subtracted from the high energy image. This dual energy subtraction technique improves the detection of contrast agent features but at the cost of adding extra noise to the image and increasing the total dose.[45]

Contrast enhanced digital mammography with monochromatic x-rays can be performed in two different ways that reduce the radiation dose compared to conventional procedures. The simplest technique that also delivers the lowest radiation dose is shown in Fig. 15(a). We display an image of a portion of the same 4.5 cm breast phantom shown in Fig. 7 obtained at 25 keV (Sn K), but at a dose of only 0.057 mGy. There are five drops of Oxilan 350,[46] an FDA-approved iodine contrast agent superimposed on the phantom in 15a. The grayscale profile to the right of the image is the measured intensity along the horizontal yellow line and shows the relative absorption of the leftmost three drops. The respective detection SNRs are noted.

Since the measurements in Fig. 15 are monochromatic, we can directly determine the average column density of the iodine. As per the nomenclature used above to calculate the SNR, the fraction of x-rays, Δ, absorbed by each drop, equals $(Nb - Nm)/Nb$ and the transmission through each drop is $1-\Delta$. The data in Fig. 15(a) yield an average column density for the three cases equal to ~4.5 mg/cm^2. At this low dose, the monochromatic system could detect iodine with a column density of 0.34 mg/cm^2 with a SNR = 3. A column density of ~0.1 mg/cm^2 could be detected with a SNR = 3 by increasing the dose to 0.65 mGy.

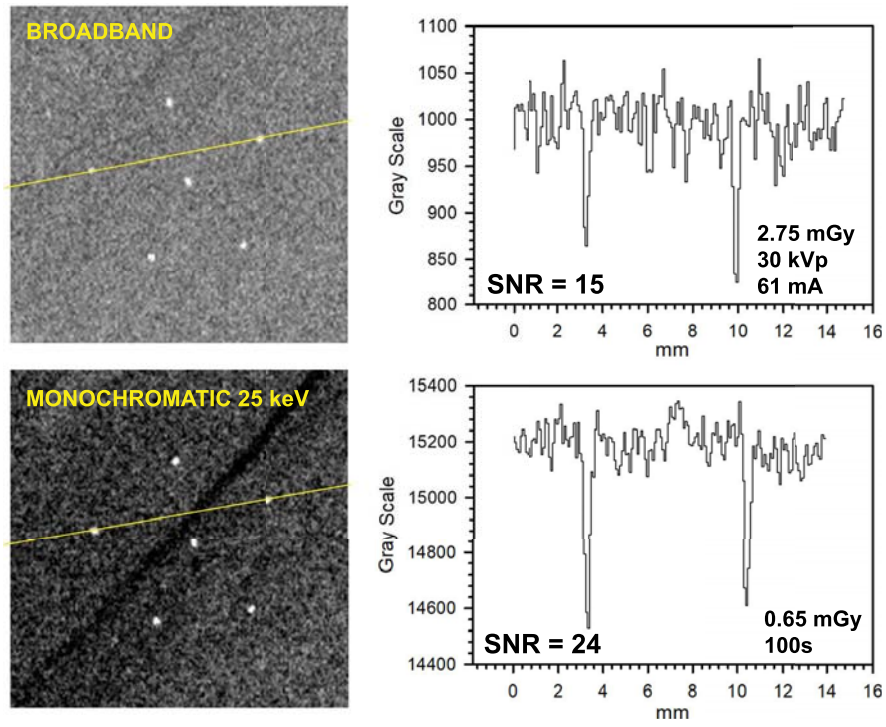

FIG. 12. The signal-to-noise ratio of the prototype at 25 keV compared to the conventional unit for 230 micron diameter microcalcifications in a 9 cm thick phantom. [Color figure can be viewed at wileyonlinelibrary.com]

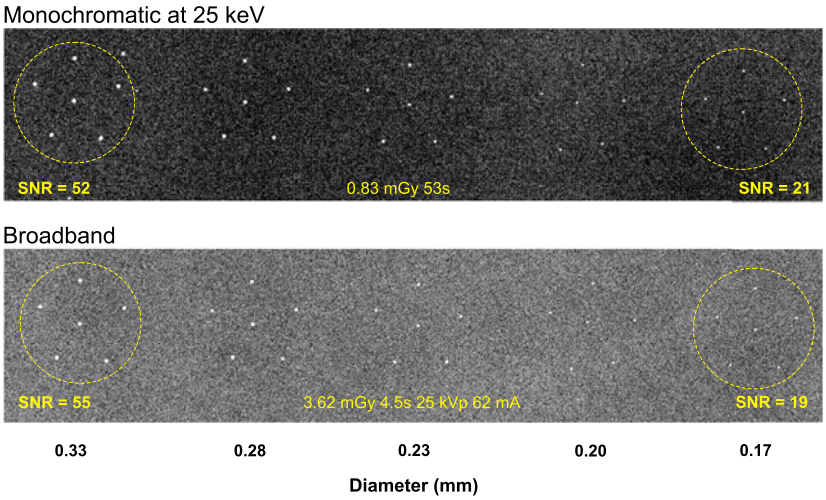

FIG. 13. The signal-to-noise ratio of the monochromatic prototype at 0.83 mGy compared to the conventional unit at 3.62 mGy for 330, 280, 230, 200, and 170 micron diameter SiO_2 simulated microcalcifications embedded in the 4.1 cm ACR086 phantom. [Color figure can be viewed at wileyonlinelibrary.com]

As mentioned above, subtracting an image with the same monochromatic spectrum but without contrast yields the difference image shown in Fig. 15(b). Although the SNR for the iodine detection in the subtracted image is reduced, the absolute contrast is unchanged and the background variations in the phantom structure have been eliminated. While this simple subtraction technique could potentially reduce tissue structure fluctuations and remove them from the iodine image, it is probably impractical as a clinical technique since it is likely difficult to accurately reposition the breast after it is decompressed for injection of the contrast agent.

Figure 16(a) shows the estimated contrast from 4 mg/cm^2 iodine in a single image as a function of monochromatic x-ray energy. As expected, the highest value is obtained using the 37 keV from a neodymium fluorescence, which is above the K-absorption edge of iodine and is an option for future measurements.

Dual energy subtraction using monochromatic x-rays can offer significant contrast improvements under the proper conditions. For different monochromatic energies, Fig. 16(b) shows the expected contrast using the dual energy technique, where a 4.5 cm compressed breast is prepared with a 4 mg/

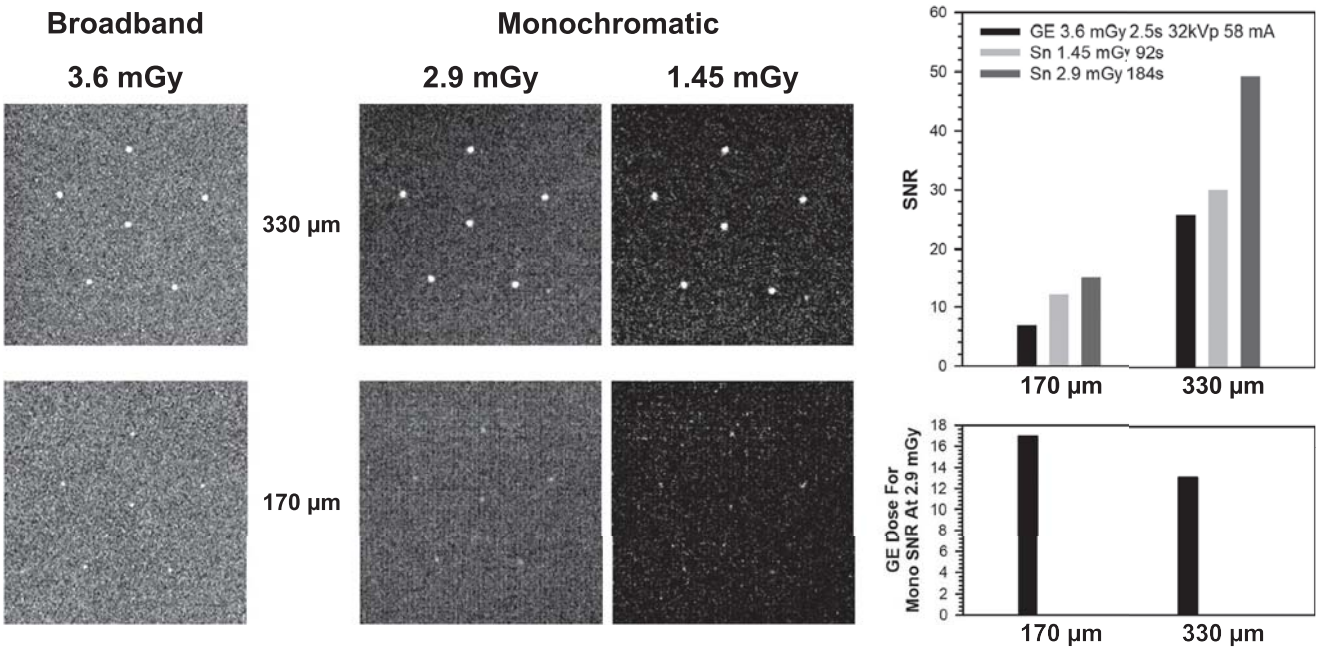

FIG. 14. The SNR of the prototype using 25 keV at 1.45 and 2.9 mGy compared to the conventional unit at 3.6 mGy for 170 and 330 micron diameter SiO_2 simulated microcalcifications in the 7.1 cm phantom. The SNR values are compared in the bar chart (top right). The extrapolated conventional doses needed to achieve the SNR values of the prototype at 2.9 mGy are also shown (bottom right).

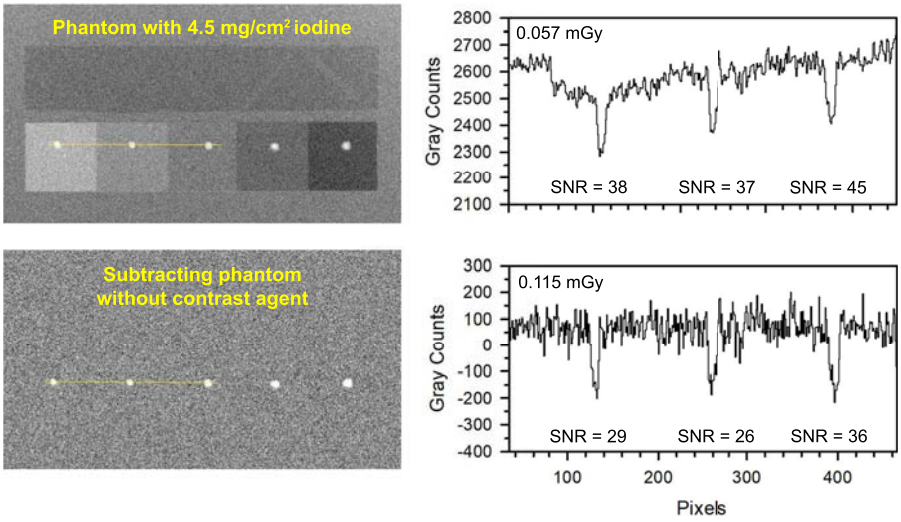

FIG. 15. Contrast-enhanced imaging with the prototype using 25 keV x-rays. (a) 4.5 cm compressed breast phantom shown with five drops of the Oxilan 350 iodine contrast agent (white dots) on top of the five step wedges. The grayscale profile to its immediate right is the intensity through the leftmost three drops. The SNR for each drop is denoted, the dose is 0.057 mGy and the exposure time was 3.4 s. (b) The consequences of subtracting a prototype image without contrast from the one in (a) with contrast. The dose increases by 2 and the SNR drops by 1.4 times as expected. [Color figure can be viewed at wileyonlinelibrary.com]

cm^2 iodine contrast drop and imaged above the iodine contrast edge with Nd x-rays at 37 keV and below the edge with a variety of monochromatic x-ray energies. Note that contrast values are dependent on the quantum absorption efficiency, QE, of the imaging detector for the two energies used in the measurements. Figure 16(b) depicts curves labeled, 50% and 85%. The calculations for the QE value of 50% correspond to the efficiency at 37 keV of the 200 micron thick amorphous selenium detector used in our mammography system. Under these conditions, the expectation that the highest contrast would be obtained by subtracting an image taken with an energy immediately below the 35 keV iodine absorption edge such as Sb (26 keV) or Sn (25 keV), where the QE is greater than 85%, is not correct nor is it much of an improvement over the contrast obtained with a single energy at 37 keV as shown in Fig. 16(a). Only subtracting an image obtained at a lower energy such as 22 keV from Ag where the absorption is dominated by the breast tissue rather than the contrast agent, does the contrast from the dual energy subtraction dramatically improve. However, as the QE of the

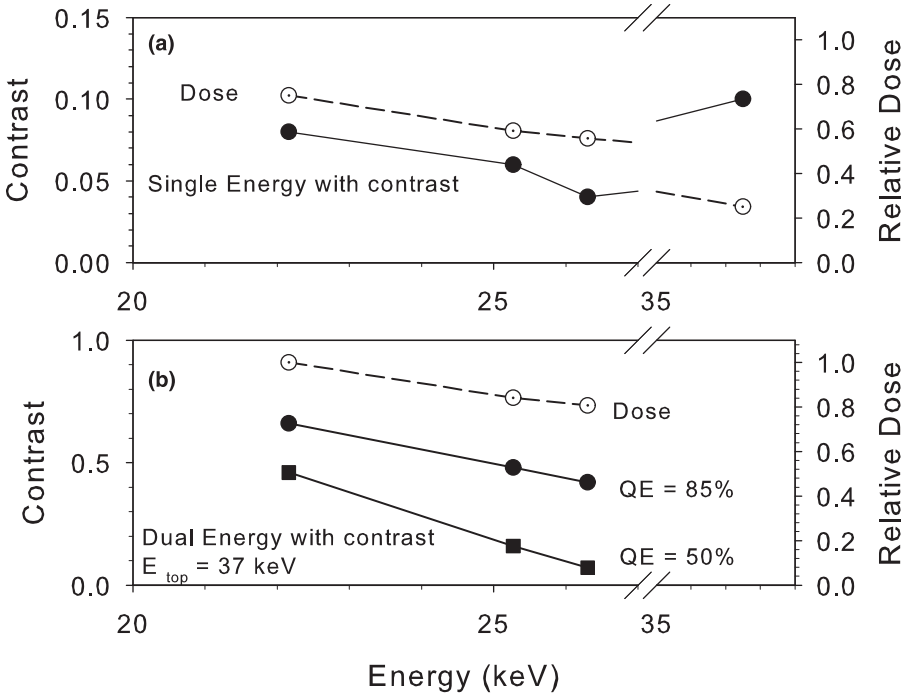

FIG. 16. The contrast expected in images obtained using contrast with a single monochromatic energy (a) and from images where dual energy subtraction was performed (b).

detector at 37 keV increases to 85%, the dual energy contrast performance at 25–26 keV also increases.

4. DISCUSSION

The performance advantages of our prototype mammography system stem from its ability to produce a monoenergetic x-ray spectrum at a selectable energy, and we expect that the extensive range of selectable monochromatic energies also enables CT, fluoroscopy, and other radiological imaging applications. The prototype produces uniform, wide field-of-view images with high image quality at low dose, all within the footprint of existing conventional mammography systems. The image comparisons above show that this monochromatic technology can reduce the radiation dose by a factor of five to ten times while still providing better image quality.

It is reasonable to assume that the comparisons of image quality between our monochromatic mammographic system, which uses the direct a-Se Analogic detector with 85 micron pixel pitch and the GE mammography machine, which uses an indirect a-Si CsI detector, are not limited, to first order, by the use of either detector type. Although the limiting resolution afforded by an 85 micron pixel is superior to a 100 micron pixel, its perceived advantage is likely less important that the SNR of the individual detector. This is evident by the comparable spatial resolution displayed in the images discussed above. It is better, therefore, to compare the detective quantum efficiency, DQE, of the detectors as a function of spatial frequency and radiation dose because the DQE accounts for the MTF response, the photon quantum efficiency and the intrinsic noise of the detector.

Comparisons of the DQE for each type of detector are found in the literature[47,48] Suffice it to say that the DQE of both detector types are similar (~50–65% at 1 lp/mm) and (30% at 5 lp/mm). We have performed a few measurements of the DQE for our a-Se detector and obtained similar results. Methods to optimize the scintillator layer of the a-Si-CsI have also been described that would increase the DQE for the a-Si-CsI by at least 15% over these values. A potentially more important finding is that the DQE of the indirect a-Si-CsI detector is superior at lower radiation dose compared to the direct a-Se imager.[48] This implies that monochromatic imaging studies using the indirect a-Si-Csi detector instead of the direct a-Se detector would further improve current performance of our monochromatic system.

Presently, the exposure times for these imaging studies are relatively long, especially for imaging thick breast tissue. They serve as benchmarks for ongoing work that will increase the monochromatic flux, thereby reducing image acquisition time. A tube with at least ten times higher power is already designed and under development. It will use the same 34 cm × 11 cm cylindrical volume as the 1.6 kW tube since the majority of the space is needed for the high voltage connection. As mentioned earlier, the geometry of the large stationary anode is ideal for higher power applications because the electron beam power is distributed over a large area in an analogous way to that of a rotating anode in a high power conventional tube. In addition, the stationary anode eliminates the cooling issues associated with heat removal through a rotating shaft. We anticipate that 1–10 s exposure times will be achieved with this tube. The design also incorporates the ability to pulse the electron beam.

Further intensity increases in monochromatic flux are available by increasing the surface area of the fluorescence target. Conical targets with base diameters of 8 mm have been tested extensively and deliver about 2.2 times the flux, but the effective spot size increases by about a factor of 2. For the 76 cm source–detector distance used in our experiments to date, the spatial resolution degrades by about 30% for 250 micron diameter microcalcifications. Of course, reducing the source–detector distance to 660 mm as in conventional mammography machines would immediately increase the flux by 33% while only degrading the spatial resolution by 5%. We point out that the present capability to image 4.5 cm compressed phantoms within 10–30 s is already compatible with tomosynthesis in this time frame using point-and-shoot scans which distribute the total dose among the individual angular measurements.

These powerful capabilities add substantial benefits and new options for screening dense and thick breasts and for diagnosing difficult cases involving small tumors or other unresolved features. They will potentially allow screening with significantly less compression while preserving detection sensitivity, thus improving patient comfort and hopefully lead to improved compliance with annual screening guidelines.

The diagnostic use of monochromatic x-ray mammography can potentially reduce unnecessary, negative biopsies and replace more expensive follow-up technologies such as MRI and MBI (Molecular Breast Imaging). As described above, monochromatic x-rays provide the ideal technology for CEDM. Contrast agents enhance the x-ray absorption in suspected lesions relative to the surrounding tissue, thereby increasing image detail and enabling visualization of cancers that are otherwise extremely difficult to detect. CEDM is receiving increased attention especially in the screening of women at high risk of developing breast cancer and as a diagnostic tool when anomalies are seen in routine screening mammograms[45,49] Monochromatic x-rays provide very high sensitivity iodine detection in a single image at a low radiation dose. The dose in the CEDM test discussed here is only 0.057 mGy, demonstrating that monochromatic x-rays enhance the potential for widespread use of CEDM while substantially reducing radiation exposure. Furthermore, monochromatic x-rays could enable dynamic studies of the rate of contrast uptake by the lesion and surrounding tissue since several images can be taken in succession while still keeping the total dose at acceptable levels.

Radiation risk is an important consideration in all imaging using ionizing radiation. Although the latest report of the United Nations Scientific Committee on Effects of Atomic Radiations (UNSCEAR) is not available, indications are that the global use of x-ray exams is around 4 to 5 billion annually, up from 3.6 billion in 2008. The breast is one of the most radiosensitive organs in the human body and consequently, the International Commission on Radiological Protection (ICRP) increased the tissue weighting factor for the breast from its moderate category of 0.05 to its most sensitive category of 0.12, an increase of a factor of 2.4.[50] An estimated 39 million mammograms are performed in the United States every year, amounting to a collective dose of 14,131 person-sieverts in 2016 alone.[1] Various authors indicate that the lifetime screening dose itself may cause 1%–2% additional cases of breast cancer.[51] Individuals with large breasts, those with certain predispositions (BRCA1/BRCA2, family history), and those who started screening at an early age could have a substantially increased risk for x-ray induced cancers.[52] The factor of 5 to 10 reduction in radiation dose per mammogram made possible by monochromatic x-rays will lead to a major reduction in total exposure from breast cancer screening and a dramatically reduced risk of radiation-induced cancers in at-risk women.

5. CONCLUSION

While dramatically reducing radiation dose in mammography examinations, monochromatic x-rays produce superior images with enhanced sensitivity. Monochromatic x-rays used at doses approaching those currently used in screening by broadband mammography systems offer additional sensitivity if follow-up diagnostics are necessary to image suspected lesions detected during screening. CEDM with monochromatic x-rays may be another alternative for superior diagnostic follow-up.

ACKNOWLEDGMENTS

The authors thank Elsie Levin, MD, Director of the Boston Breast Diagnostic Center, for allowing us to use its conventional, broadband commercial mammography machines to make measurements.

Funding for this work was supported entirely by Imagine Scientific, Inc.

CONFLICT OF INTEREST

Eric H. Silver is the Founder and CEO of Imagine Scientific, Inc. Seth D. Shulman is a consultant to Imagine Scientific, Inc. and a shareholder. Madan M. Rehani is the Director of Global Outreach for Radiation Protection in the Radiology Department at the Massachusetts General Hospital and is an unpaid collaborator.

[a]Author to whom correspondence should be addressed. Electronic mail: eric.silver@imaginescientific.com.

REFERENCES

1. Mettler FA Jr, Mahesh M, Bhargavan-Chatfield M, et al. Patient exposure from radiologic and nuclear medicine procedures in the United States: procedure volume and effective dose for the period 2006–2016. *Radiology*. 2020;295:418–427.
2. Rehani MM, Yang K, Melick ER, et al. Patients undergoing recurrent CT scans: assessing the magnitude. *Eur Radiol*. 2020;30:1828–1836.
3. Brambilla M, Vassileva J, Kuchcinska A, Rehani MM. Multinational data on cumulative radiation exposure of patients from recurrent radiological procedures: call for action. *Eur Radiol*. 2020;30:2493–2501.

4. Rehani MM, Melick ER, Alvi RM, et al. Patients undergoing recurrent CT exams: assessment of patients with non-malignant diseases, reasons for imaging and imaging appropriateness. *Eur Radiol*. 2020;30: 1839–1846.
5. Rehani MM. Challenges in radiation protection of patients for the 21st century. *AJR Am J Roentgenol*. 2013;200:762–764.
6. Clark GL. Medical, biological and industrial applications of monochromatic radiography and microradiography. *Radiology*. 1947;49:483–495.
7. Ter-Pogossian M. Monochromatic roentgen rays in contrast media roentgenography. *Acta Radiol*. 1956;45:313–322.
8. Oosterkamp IW. Monochromatic X-rays for medical fluoroscopy and radiography. *Medicamundi*. 1961;7:68–77.
9. Carroll F. Use of monochromatic x-rays in medical diagnosis and therapy what is it going to take? *J X-ray Sci Technol*. 1994;4:323–333.
10. Hoheisel M, Lawaczeck R, Pietsch H, Arkadiev V. Advantages of Monochromatic X-rays for Imaging. Medical Imaging: Physics of Medical Imaging, edited by Michael J. Flynn, Proceedings; 2005.
11. Sugiro FR, Li D, MacDonald CA. Beam collimation with polycapillary x-ray optics for high contrast high resolution monochromatic imaging. *Med Phys*. 2004;31:3288–3397.
12. Rubenstein E, Brown GS, Harrison DC, et al. Synchrotron radiation for transvenous coronary angiography. *Trans Am Clin Climatol Assoc*. 1986;97:27–31.
13. Tokumori K, Toyofuku F, Kanda S, et al.Monochromatic X-ray CT using fluorescent X-rays excited by synchrotron radiation, Engineering in Medicine and Biology Society. Proceedings of the 22nd Annual International Conference of the IEEE; 2000; 4: 2987–2989.
14. Burattini E, Cossu E, Di Maggio C, et al. Mammography with synchrotron radiation. *Radiology*. 1995;195:239–244.
15. Arfelli F, Bonvicini V, Bravin A, et al. Mammography of a phantom and breast tissue with synchrotron radiation and a linear-array silicon detector. *Radiology*. 1998;208:709–715.
16. Kulpe S, Dierolf M, Braig E, et al. K-edge subtraction imaging for coronary angiography with a compact synchrotron X-ray source. *PLOS ONE*. 2018;13:e0208446.
17. Yoon K-H, Kwon YM, Choi B-J, et al. Monochromatic X-rays for low-dose digital mammography. *Prelim Result Invest Radiol*. 2012;47:683–687.
18. Windt DL. Monochromatic mammography using scanning multilayer mrrors. *Rev Sci Instrum*. 2018;89:083702.
19. X-123CdTe, Amptek Inc. 14 Deangelo Dr, Bedford, MA 01730.
20. Attix, Frank Herbert. Intro to Radiological Physics and Radiation Dosimetry, Wiley-VCH Verlag GmbH & Co. KGaA, 1986.
21. Storm E. Bremsstrahlung-induced K-fluorescent radiation. *J Appl Phys*. 1976;47:3060.
22. Silver EH. Monochromatic X-ray Methods and Apparatus, *U.S. Patent* 8331354; 2012.
23. Silver EH. Monochromatic X-ray Methods and Apparatus, *U.S. Patent*, 9066702; 2015.
24. Silver EH. Monochromatic X-ray Methods and Apparatus, *U.S. Patent* 9326744; 2016.
25. Silver EH. Monochromatic X-ray Methods and Apparatus, *U.S. Patent*, 10299743; 2019.
26. Silver EH. Monochromatic X-ray Systems and Methods, *U.S. Patent* 10398909; 2019.
27. Silver EH. Monochromatic X-ray Imaging Systems And Methods, *US Patent* 10398910; 2019.
28. Silver EH. Monochromatic X-ray Imaging Systems And Methods, *US Patent* 10532223; 2020.
29. Silver EH. Monochromatic X-ray Systems And Methods, *US Patent* 10806946; 2020.
30. Silver EH. Monochromatic X-ray Systems And Methods, *US Patent* 10857383; 2020.
31. Silver EH. Methods and Apparatus for Determining Information Regarding Chemical Composition Using X-radiation, *U.S. Patent Application Pub. No.: US 2018/0284036 A1*; 2018.
32. Analogic Canada Digital Mammography, 4950 Levy Street, Saint-Laurent, Québec, Canada, H4R 2P1.
33. Illers H, Buhr E, Gunther-Kohfahl S, Neitzel U. Measurement Of The Modulation Transfer Function Of Digital X-ray Detectors With An Opaque Edge-Test Device, Radiation Protection Dosimetry; 2005, Vol. 114, Nos 1-3, pp. 214–219. https://doi.org/10.1093/rpd/nch506
34. International Electrotechnical Commission. Medical electrical equipment—Characteristics of digital X-ray imaging devices—Part 1: determination of the detective quantum efficiency. IEC 62220-1 (Geneva: IEC); 2003.
35. GE Medical Systems.Senographe Essential VERSION ADS_54.20.
36. Computerized Imaging Reference Systems Inc. 900 Asbury Ave., Norfolk, VA 23513, USA.
37. Dance DR. Monte Carlo calculation of conversion factors for the estimation of mean glandular breast dose. *Phys Med Biol*. 1990;35:1211–1219.
38. Dance DR, Young KC, van Engen RE. Further factors for the estimation of mean glandular dose using the United Kingdom, European and IAEA breast dosimetry protocols. *Phys Med Biol*. 2009;54:4361–4372.
39. Sobol WT, Wu X. Parametrization of mammography normalized average glandular dose tables. *Med Phys*. 1997;24:547–554.
40. Wu X, Gingold EL, Barnes GT, Tucker DM. Normalized average glandular dose in molybdenum target-rhodium filter and rhodium target-rhodium filter mammography. *Radiology*. 1994;193:83–89.
41. Boone JM. Glandular breast dose for monoenergetic and high-energy X-ray beams: Monte Carlo assessment. *Radiology*. 1999;213:23–37.
42. Boone JM. Normalized glandular dose (DgN) coefficients for arbitrary X-ray spectra in mammography: computer-fit values of Monte Carlo derived data. *Med Phys*. 2002;29:869–875.
43. Okunade AA. Method for the evaluation of a average glandular dose in mammography. *Med Phys*. 2006;33:1153–1164.
44. Suleiman ME, Brennan PC, McEntee MF. Mean glandular dose in digital mammography: a dose calculation method comparison. *J Med Imaging (Bellingham)*. 2017;4:013502.
45. Phillips J, Miller MM, Mehta TS, et al. Contrast-enhanced spectral mammography (CESM) versus MRI in the high-risk screening setting: patient preferences and attitudes. *Clin Imaging*. 2017;42:193–197.
46. Guerbet LLC. 821 Alexander Road, Suite 204, Princeton, NJ 08540.
47. Albagli D, Hudspeth H, Possin GE, et al. Performance of advanced a-Si/CsI-based flat panel x-ray detectors for mammography. *Proc SPIE*. 2003;5030:553.
48. Shaw J, Albagli D, Wei C-Y, Granfors PR. Enhanced a-Si/CsI-based flat-panel X-ray detector for mammography. Proc. SPIE 5368, Medical Imaging 2004: Physics of Medical Imaging, (6 May 2004). https://doi.org/10.1117/12.539141
49. Lewis TC, Patel BK, Pizzitola VJ. Navigating Contrast-enhanced Digital Mammography. *Appl Radiol*. 2017;46(3):21–28. https://appliedradiology.com/articles/navigating-contrast-enhanced-digital-mammography
50. ICRP. The 2007 Recommendations of the International Commission on Radiological Protection, ICRP Publication 103. Ann. ICRP 37 (2–4); 2007.
51. Miglioretti DL, Lange J, van den Broek JJ, et al. Radiation-induced breast cancer incidence and mortality from digital mammography screening: a modeling study. *Ann Intern Med*. 2016;164:205–214.
52. Pauwels EK, Foray N, Bourguignon MH. Breast cancer induced by x-ray mammography screening? A review based on recent understanding of low-dose radiobiology. *Med Princ Pract*. 2016;25:101–109.